

# Development of Spatial Optical Coherence Tomography Methods to Characterize Thin Biological Samples

A Major Qualifying Project Report  
submitted to the Faculty  
of the

WORCESTER POLYTECHNIC INSTITUTE

In Partial Fulfillment of the requirements for the

Degree of Bachelor of Science

By

Stephen Couitt

---

Stephan Montañez-Sanchez

---

Date: 4/28/2015

Approved:

Professor Cosme Furlong, Advisor

Professor Germano Iannacchione, Co-Advisor

This report represents the work of WPI undergraduate students submitted to the faculty as evidence of completion of a degree requirement. WPI routinely publishes these reports on its website without editorial or peer review. For more information about the projects program at WPI, please see <http://www.wpi.edu/academics/ugradstudies/project-learning.html>

## Abstract

Obtaining thicknesses of micro-scale samples through noninvasive methods is crucial when dealing with fragile or biological samples. Optical Coherence Tomography (OCT) is an imaging technique which uses low coherence interferometry to create a layered stack of cross-sectional images without directly contacting the sample. From the interference patterns in the obtained images, surface, internal structures and their locations can be computationally calculated and a three dimensional representation of the sample can be rendered.

The OCT setup that was developed for our experimentation utilized a 780nm light source imaged with a Pike F145-B camera and a Leica HCX PL FLUOTAR 5x/0.15 Michaelson interferometer attached to a P-7254CL 400 $\mu$ m travel piezo to ensure that both top and bottom surfaces were imaged, and the image processing was done in Matlab, which yielded the surface and internal structures. To test the accuracy of our OCT setup, non-biological samples of known thickness were both measured to corroborate thickness and then imaged resulting in an average  $\pm 4.73\%$  difference from the known thickness values. With the accuracy of the system known, thin biological samples were then imaged and their internal structures were observed and compared to known data in order to validate the results.

## Acknowledgements

We would like to offer our thanks to Morteza Khaleghi, Payam Razavi, Koohyar Pooladvand, and other members of the CHSLT lab. Also to John Rosowski, Tao Cheng, Mike Ravicz, and all other members of the MEEI, and our advisors Cosme Furlong and Germano Iannacchione. The CHSLT labs for letting us use their equipment. Which without all their help this project would not have been possible to complete.

# Table of Contents

Abstract.....	2
Table of Contents.....	4
Table of Figures.....	6
1.0 Introduction.....	7
2.0 Background.....	9
2.1 Interferometry.....	9
2.2 Optical Coherence Tomography.....	14
2.2.1 Time Domain.....	16
2.2.2 Frequency Domain.....	16
2.2.3 Spatial Domain.....	16
2.2.4 Spatial OCT Mathematics.....	17
2.3 OCT Terminology.....	20
3.0 Methodology.....	22
3.1 Optical Coherence Tomography Setup.....	22
3.1.1 Light Source.....	22
3.1.2 Piezo.....	24
3.1.3 Objective.....	25
3.1.4 Camera.....	27
3.2 Procedure.....	29
3.2.1 Sample Preparation.....	29
3.2.2 Image Acquisition.....	30
3.2.3 Image Processing.....	30
4.0 Validation.....	31
5.0 Biological Samples.....	41
5.1 Internal Epidermal Onion Tissue.....	42
5.2 Celery Stalk.....	45
6.0 Conclusions.....	47
7.0 Future Work.....	47
References.....	49

Appendix .....	51
Single Pixel Code.....	51
Full 3D Code.....	52
Labview Code .....	56

## Table of Figures

Figure 1: Illustration of a Michelson interferometer (Boeglin, 2011).....	10
Figure 2: Resulting interference of light waves due to varying initial phase.....	12
Figure 3: Phase shift of $\Delta\phi$ between two identical waves. ....	13
Figure 4: Schematic drawing of a spatial OCT setup using a Michelson interferometer.....	15
Figure 5: Example of image acquisition from a spatial OCT system. ....	17
Figure 6: Thorlabs 780L3 LED normalized intensity versus wavelength plot. ....	23
Figure 7: Geometric optics for a simple lens. ....	25
Figure 8: Spectral response of the Pike F145-B for overall and individual color relative to wavelength...	28
Figure 9: Spectral response of the Pike F100-B for individual color relative to wavelength.....	28
Figure 10 Roscolux scarlet color filter technical data sheet used.....	32
..... Figure 11: Recorded interference pattern for 2 surfaces of a Scarlet Roscolux color swatch. ....	33
Figure 12: Measured Scarlet Roscolux color swatch thickness map plot showing both surfaces.....	34
Figure 13: Measured B-Scan of a Scarlet Roscolux color swatch.....	35
Figure 14: Measured 3-dimensional figure of a Scarlet Roscolux color swatch of both .....	36
Figure 15: Roscolux Gaslight Green color filter technical data sheet used. ....	37
Figure 16: Roscolux Tough Plusgreen color filter technical data sheet used. ....	38
Figure 17: Roscolux Cerulean Blue color filter technical data sheet used.....	39
Figure 18: Measured intensity distribution of a Cerulean Blue Roscolux.....	40
Figure 19: An A-Scan of an inner epidermal layer of an onion sample.....	43
Figure 20: A-Scan of an inner epidermal layer of an onion sample depicting cell boundaries. ....	45
Figure 21: An A-Scan of a celery stalk sample with internal structures visible. ....	46

## 1.0 Introduction

The study of fragile samples, especially biological ones, is difficult to accomplish without potentially damaging the specimen under investigation. Damaging and even the destruction of the sample must occur for some imaging techniques and in cases where the sample is not readily available in large quantities, performing a comprehensive experiment can be difficult. Because of this, a technique with which study of such samples can be done without potentially damaging or destroying the specimen is needed. Optical Coherence Tomography (OCT) is an optical technique that can do this while maintaining a high level of accuracy and with sub-micron resolution. With this technique, quantitative 3-dimensional representations can be made of the sample for further study.

Optical Coherence Tomography is a very hot topic in the scientific community for current research. It's an extremely useful technique that allows for the study of both biological and non-biological samples in a non-invasive way. This imaging technique follows the principles of white light interferometry. What this means is that it uses the superposition of light waves to determine where interference occurs. With knowledge of the interference patterns, peak intensities can be found, which corresponds to the location of highest reflectivity in the sample, essentially a surface.

OCT is very similar to ultrasound, which means it has many terms that are similar or even analogous to it. The analogy here being OCT is to light as ultrasound is to sound. Similar to ultrasound, the sample has to have good properties related to the scanning source, in OCT this would be the light source used. A high reflectivity and transmissivity is desired, with low levels of absorption, which would enable the light source to penetrate through the entire thickness of the sample.

OCT also has several imaging modalities, each having different strengths and weaknesses. The main modalities being: Time Domain, Frequency Domain, and Spatial Domain. There are additional imaging modes; however they are a combination of one or more of these.

Our goal was to build a Spatial Domain OCT system in which thickness and internal structures of samples, both biological and not, can be studied. After its construction, a validation of its capabilities to ensure it met the necessary requirements was done. Once the accuracy of the system was determined, biological samples could then be imaged so that both their thickness and internal structures were able to be studied.

## 2.0 Background

The goal of this Chapter is to provide background information that is crucial for understanding how optical coherence tomography operates and what fundamental techniques make up this imaging method. It begins with describing interferometry and how electromagnetic radiation can interfere either constructively or destructively. Coherence length is defined and its importance is explained. With the basic principles that make up OCT possible explained, the different types of OCT are explained. Due to the fact that spatial OCT will be used for the experimentation further clarification of this method is explained along with the fundamental mathematics which it utilizes. The final aspect which is explained in this section consists of OCT terminology which will be referred to throughout the report.

### 2.1 Interferometry

Interferometry is an optical technique in which the superposition of a split and then recombined light source is used to gather information. A general interferometer consists of a light source which is sent through a beam splitter. A 50-50 beam splitter allows half of the incoming light to be transmitted through and reflects the other half. When this beam splitter is set to be 45 degrees from the incoming light, the resulting split light beams are tangent to each other (Bennett, 2008). As shown in Figure 1, one of these tangential beams travels to a mirror distance  $L_1$  away and is reflected back to the beam splitter, this is referred to as the reference beam. The other beam travels to another surface distance  $L_2$  away by which light is also reflected back to the beam splitter, this is often called the object beam.

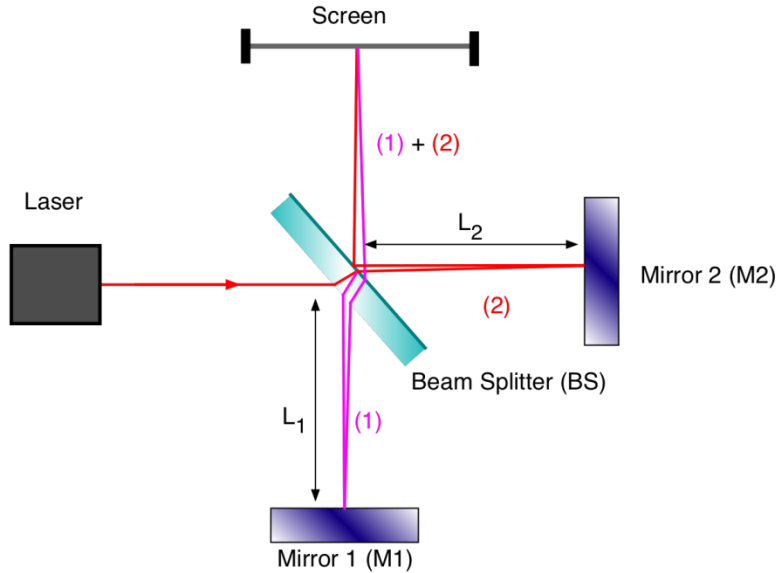


Figure 1: Illustration of a Michelson interferometer (Boeglin, 2011).

When the reference and object beams reach the splitter they are recombined. By recombining the reference and object beams a superposition of the two waves is obtained and interference will occur (Brezinski, 2006). This superposition of the reference and object beam meet at the screen where an interference pattern is visible.

For interference to occur, different light waves must travel within the same space. Like in the interferometer shown in Figure 1, the reference and object beams are recombined so that they overlap, thus producing a superposition of the two beams. When two light waves are superimposed, they interfere either constructively or destructively. The factor that determines whether the interference is constructive or destructive is the phase angle between the two waves. Phase is measured in degrees or radians, thus one wavelength of a propagating wave is equal to  $2\pi$  radians. The phase of a light wave describes the characteristics of the wave as it propagates in a medium. Phase angle of a traveling wave is most commonly represented as

$$\varphi = (kx - \omega t), \tag{1}$$

where  $k$  is the wavenumber ( $k = 2\pi/\lambda$ ) and  $\omega$  is the angular frequency ( $\omega = 2\pi f$ ) (Quimby, 2006). The phase of a wave represents oscillations both in time and spatial domains. If the relations for wavenumber and angular frequency are substituted into Eq. 1, it is apparent that phase angle is dimensionless (radians) and consists of two separate domains thus resulting in

$$\varphi = 2\pi\left(\frac{x}{\lambda} - ft\right).$$

Therefore, when it is said two adjacent light waves are traveling in phase relative to the other, they have  $\Delta\varphi = \varphi_2 - \varphi_1 = 0$ . When in phase, their amplitudes will constructively interfere, resulting in an observed wave having an amplitude equal to the sum of the two propagating waves. Destructive interference on the other hand occurs when the two waves are out of phase,  $\Delta\varphi \neq 0$ , therefore decreasing the amplitude of the observed wave, resulting in a superposition with a lower maximum than what is observed from constructive interference. When  $\Delta\varphi = \pi$ , the resulting amplitude is a minimum equal to the difference in amplitude of the two contributing waves (Sutter and Davidson, 2014). Both constructive and destructive interference are visualized in Figure 2 which shows the resulting superposition caused by waves with various initial phase angle conditions.

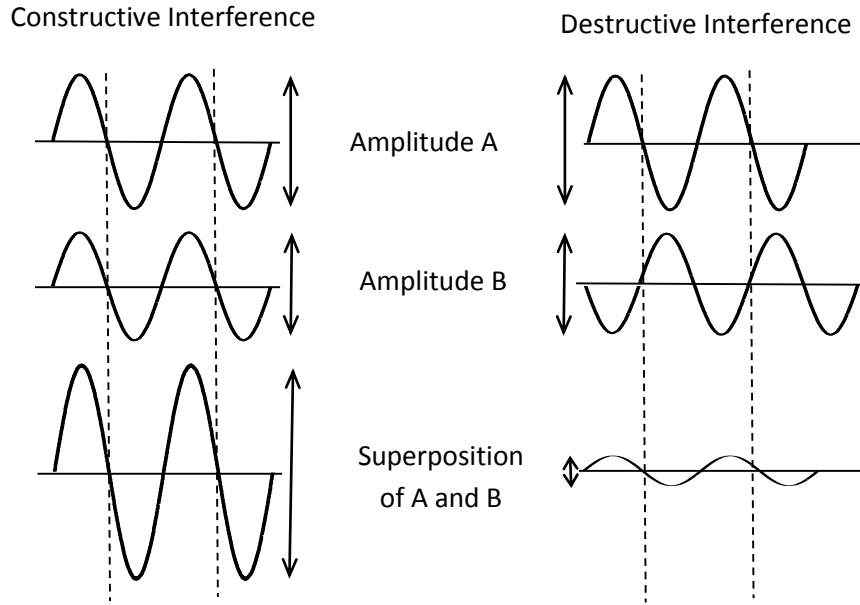


Figure 2: Resulting interference of light waves due to varying initial phase.

Electromagnetic waves can be represented by Maxwell's equations in a uniform medium where the electric field vector can be written as

$$\mathbf{E} = \mathbf{E}_0 e^{i(\varphi)},$$

and the intensity  $\mathbf{E}_T$  of the resulting superpositioned wave at a given point is determined by the amplitude of both waves (intensity is the square of the amplitude),  $\mathbf{E}_1$  and  $\mathbf{E}_2$ , given by the vector sum

$$\mathbf{E}_T = \mathbf{E}_1 + \mathbf{E}_2.$$

In the case of an interferometer, the source of the two beams is the same which means the wavelength, initial phase and intensity are identical. Therefore, the interference is determined by the phase difference,  $\Delta\Phi$ , of the two waves. Phase difference is determined by

$$\Delta\Phi = \Phi_2 - \Phi_1 = 2(L_2) - 2(L_1) = 2\Delta L,$$

where  $L_1$  and  $L_2$  are the path lengths from the beam splitter to the mirror. This phase difference is shown in Figure 3, the greater the change in the path lengths, the greater phase difference and therefore determining the type of interference that occurs.

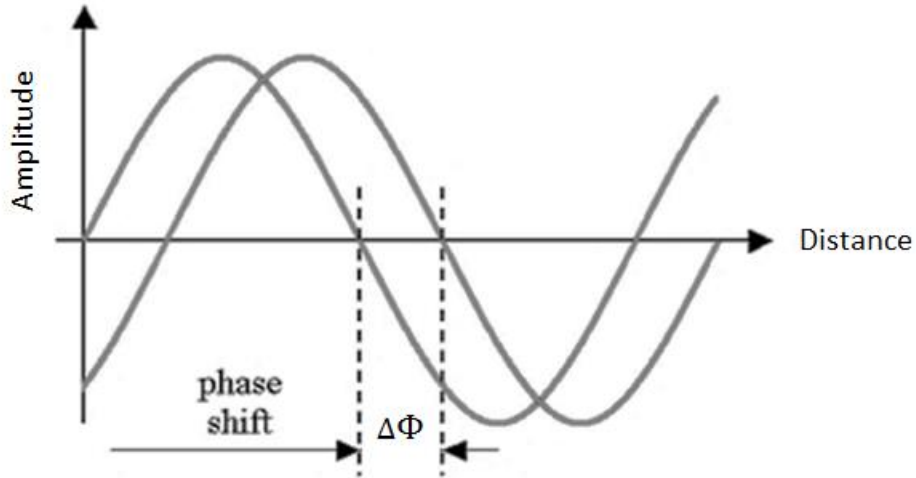


Figure 3: Phase shift of  $\Delta\Phi$  between two identical waves.

In the case of the Michelson interferometer being used, interference of light waves can only occur when the distance between the reference arm and sample are within the coherence of the light source being used. The coherence length is the difference in distance travelled by separate light waves that will cause interference to occur when they are combined (Mahadevan, 2008). Low coherence is desired for OCT because it allows quantification of distance, but high coherence is generally desired for holography. For interference to occur in a Michelson interferometer,

$$\text{Source Coherence Length} > |L_2 - L_1|, \quad (2)$$

where  $L_1$  and  $L_2$  are the lengths of the reference and objective beam respectively and the *Source Coherence Length* is a constant defined by the light source being used. The best scenario would

be when  $L_2 - L_1$  is equal to 0, which describes the situation with a well calibrated interferometer measuring a relatively flat surface.

## 2.2 Optical Coherence Tomography

OCT is an imaging system very similar to ultrasound; however it uses light instead of sound. Low intensity, typically near infrared light, is sent to the object, and a portion of that light is reflected and captured by sensors. This reflected light can then be made into an image showing thickness and internal structures of the scanned object.

In contrast to ultrasound, OCT is a noninvasive imaging technique and does not require any mechanical interaction with the sample, making it very useful for fragile or other samples in which vibrations would not be desired otherwise. As shown in Figure 4, only light interacts with the sample leaving it unharmed. Another difference between these is the level of detail that can be obtained. Since light waves are shorter than sound waves, OCT imaging allows greater detail than ultrasound. On the other hand, ultrasound can be used to image deeper into tissue, and can sometimes observe structures that are optically opaque.

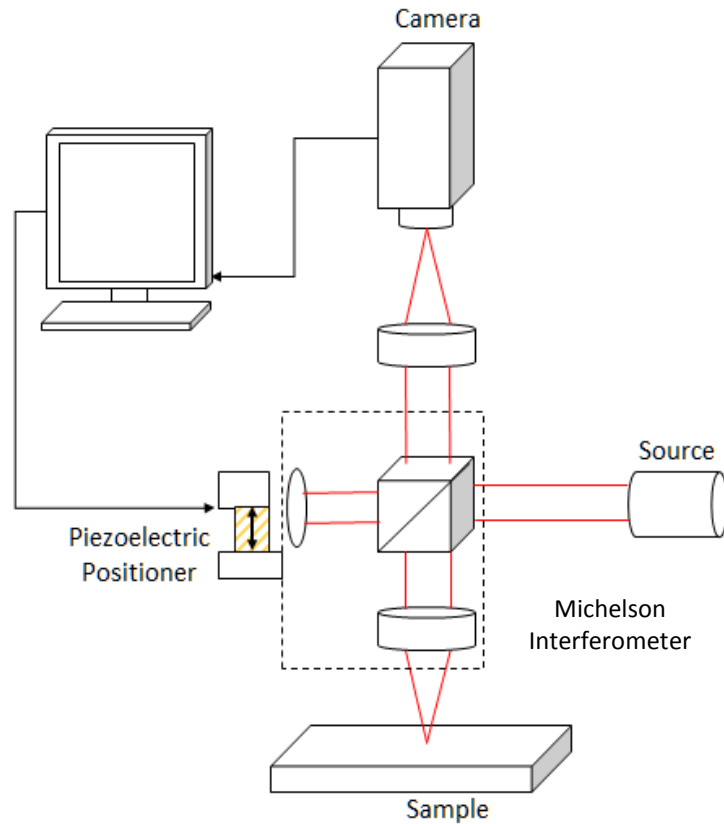


*Figure 4: Schematic drawing of a spatial OCT setup using a Michelson interferometer.*

OCT is a broad term that encompasses several methods of image acquisition and analysis, the most common including: Time Domain, Frequency Domain, and Spatial Domain. These three methods are the basis for all other variations of OCT which consist of combinations of these analysis schemes. All three have the ability to generate 3-dimensional representations of samples while providing nanometer ranged spatial resolution while also all being based on low coherence light interferometry. The method that was selected to be used in this project is Spatial Domain OCT (Huang et al., 1991; Schmitt, 1999).

### 2.2.1 Time Domain

How Time Domain OCT operates is by translating the path length of the reference arm longitudinally through time, this changes the coherence length of the system. This change causes the plane at which the interference patterns occur to change, resulting in the desired imaging step. The rate at which the path length is translated is controlled resulting in accurate known measurements of the scan time (Huang et al., 1991).

### 2.2.2 Frequency Domain

In Frequency Domain OCT the broadband interference is acquired with spectrally separated detectors. This is done by either encoding the optical frequency in time with a spectral scanning source or with a dispersive detector. The depth scan can be calculated through the Fourier-transform of the acquired spectra with no movement of the reference arm (Schmitt, 1999).

### 2.2.3 Spatial Domain

Spatial Domain OCT is performed by scanning a sample with an interferometric objective lens. This method keeps the distance between reference and sample beams fixed within the coherence length of the light source, ensuring that interference will occur when light is reflected off a surface. As the objective is stepped a fixed distance towards the sample, images are acquired cutting the sample into parallel planes. Figure 5 displays how the microscope objective is moved and how layers of images are stacked. From these images, surface and internal information can be observed based on the resulting interference patterns (Huang et al., 1991; Larkin, 1996).

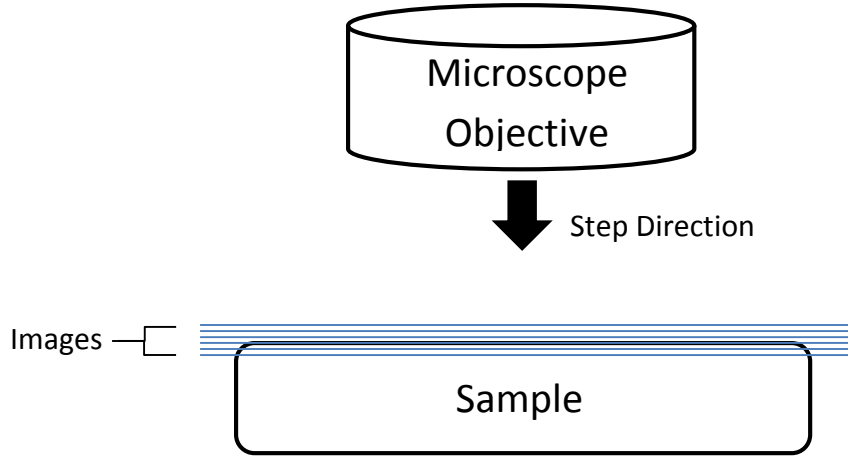


Figure 5: Example of image acquisition from a spatial OCT system.

#### 2.2.4 Spatial OCT Mathematics

Spatial Domain OCT follows the principles of white light interferometry (Larkin, 1996). In doing so, we can represent the intensity modulation of interfering light waves by the following equation

$$I_1(x, z) = A \exp\left(\frac{-[z-z_1]^2}{\sigma^2}\right) \cos\left(4\pi \frac{z}{\lambda}\right) + n(x, z), \quad (3)$$

where  $A$  is the amplitude of the intensity modulation,  $\sigma$  is the standard deviation of the intensity modulation which is related to the coherence length of the light source,  $\lambda$  is the wavelength of the light source,  $z$  is the total depth of the axial direction being scanned,  $z_1$  is the location of the maxima of the intensity modulation, and  $x$  corresponds to displacements perpendicular to depth due to Gaussian-distributed random noise.  $n(x, z)$  is Gaussian-distributed random noise, which is caused by error from the environment and acquisition procedures. For this to be true, the intensity modulation has to be within the coherence length of the light source which is defined in Eq. 3.

This same intensity modulation equation can be used in intensity modulations with more than one mode. This is accomplished by performing a summation of the intensity modulations which results in

$$I(x, z) = I_1(x, z) + I_2(x, z) . \quad (4)$$

From Eq. 4,  $I_2(x, z)$  is defined as

$$I_2(x, z) = A \exp\left(\frac{-[z-z_2]^2}{\sigma^2}\right) \cos\left(4\pi \frac{z}{\lambda}\right) + n(x, z),$$

where the only difference between  $I_1$  and  $I_2$  is  $z_2$ , which is a different maxima location than  $z_1$ . Keeping in mind however, in many cases the amplitude of the second modulation is smaller than the firsts', this is due to loss of intensity from the light traveling through the sample.

These equations represent the intensity modulation properly, however even with them it is a simple task to locate the corresponding “peak” or maximum value which would correspond to the position of greatest intensity. In order to do this, an “envelope” needs to be used on the intensity modulation. What this envelope does is essentially cover the modulation which would in turn allow for much easier peak detection. This is accomplished by using the Hilbert transformation of the intensity modulation.

A Hilbert transform adds a phase shift of  $\pi/2$  to a Fourier function. The Hilbert transform begins by using the intensity modulation defined as

$$f(z) = \exp\left(\frac{-[z-z_1]^2}{\sigma^2}\right) \cos\left(4\pi \frac{z}{\lambda}\right). \quad (5)$$

When in the frequency domain, Eq. 5 undergoes a  $\pi/2$  phase shift, which yields

$$f'(z) = \exp\left(\frac{-[z-z_1]^2}{\sigma^2}\right) i \sin\left(4\pi \frac{z}{\lambda}\right). \quad (6)$$

To generate the envelope Eqs. 5 and 6 are added and represented in a complex representation, which means that they contain real and imaginary components. Thus, the representation of the envelope is

$$F(z) = f(z) + f'(z). \quad (7)$$

When Eqs. 5 and 6 are substituted into Eq. 7, it is obtained

$$F(z) = \exp\left(\frac{-[z-z_1]^2}{\sigma^2}\right) [\cos\left(4\pi \frac{z}{\lambda}\right) + i \sin\left(4\pi \frac{z}{\lambda}\right)], \quad (8)$$

and by computing the magnitude of Eq. 8,

$$|F(z)| = \sqrt{\exp\left(\frac{-[z-z_1]^2}{\sigma^2}\right)^2} \sqrt{[\cos\left(4\pi \frac{z}{\lambda}\right)]^2 + [\sin\left(4\pi \frac{z}{\lambda}\right)]^2}, \quad (9)$$

is obtained. Through trigonometry's Euler's Identity this can be simplified further. Euler's Identity being

$$\cos(x)^2 + \sin(x)^2 = 1 \quad (10)$$

and by applying Eq. 10 to Eq. 9,

$$|F(z)| = \left| \exp\left(\frac{-[z-z_1]^2}{\sigma^2}\right) \right| \quad (11)$$

is obtained. Equation 11 is the envelope used to locate the peaks in the previous intensity modulation equations. As well as for single peak detection, the Hilbert transform can be used for multi-peak or multi-modal intensity modulations.

## 2.3 OCT Terminology

Because OCT is analogous to ultrasound in that both are based on measuring the delay of a reflected wave, there are terminologies which are similar in name and feature for both imaging method. In ultrasound, A-Scan refers to the oscilloscope display where the vertical dimension is used to display amplitude and the horizontal dimension represents the echo delay (depth). In OCT, A-Scan can also be taken as the abbreviation for axial scan, representing reflected optical amplitude along the axis of light propagation. Ultrasound B-Scan referred to the cathode ray tube display where the brightness represents the amplitude of echoes. In OCT, a B-Scan refers to the cross-sectional image where the amplitudes of reflections are represented in a gray scale or a false-color scale. In ultrasound, a C-Scan refers to a section across structures at an equal echo delay. In OCT, a C-Scan refers to a section across structures at an equal optical delay (Huang, 2009).

To obtain these A-Scans and B-Scans we must use the “intensity modulation” equations given by:

$$I_1 = I_0 * [1 + \gamma * \cos(\Phi - \alpha)], \quad (12)$$

$$I_2 = I_0 * [1 + \gamma * \cos(\Phi)], \quad (13)$$

$$I_3 = I_0 * [1 + \gamma * \cos(\Phi + \alpha)], \quad (14)$$

$$I_4 = I_0 * [1 + \gamma * \cos(\Phi + 2\alpha)], \quad (15)$$

$$\gamma = \frac{\sqrt{(I_3 - I_2)^2 + (I_1 - I_2)^2}}{\sqrt{2} * I_0}, \quad (16)$$

$$I_0 = \frac{I_1 + I_2 + I_3 + I_4}{4}, \quad (17)$$

where  $I_n$  represents intensity,  $\gamma$  is the “intensity modulation”,  $\Phi$  is the phase, and  $\alpha$  is the phase shift, which in our case was taken to be  $\pi/2$ .

With Eqs. 12 through 17, a captured intensity modulation is used to calculate the  $\gamma$  which is the value of interest. This is possible because the intensity values at each position are known and from them, other equations can be derived so that the unknown values can be solved for.

## 3.0 Methodology

For this project, the goal is to develop a spatial domain optical coherence tomography setup as a measurement tool to acquire thickness and internal structures of samples. This Section will outline the setup that was used and the reasons each part was selected over other options that were available. Once the setup is fully described, the procedure of how images were obtained will be defined along with how they were processed. Next the validation of the accuracy of the OCT setup will be reviewed in detail. All of these then contribute to the overall process of biological sample selection and imaging.

### 3.1 Optical Coherence Tomography Setup

The Optical Coherence Tomography setup that was used in this experimentation consists of four main devices, a light source, a piezoelectric microscope objective positioner, an interferometric microscope objective, and a camera.

#### 3.1.1 Light Source

As mentioned in the background, coherence length is dependent on the source of light used, with shorter wavelengths resulting in higher accuracy imaging. For this project, light sources ranging from near violet to infrared were available in the form of LED diodes. The source that was selected was the 780nm near infrared diode from Thorlabs, whose specifications are shown in Table 1. Nominal wavelength and the power outputs being the items of greatest interest for the system. In Figure 6 a distribution of the normalized intensity versus the

wavelength is plotted showing the operating wavelengths produced from the 780 nm diode source.

Table 1: Thorlabs 780L3 LED specifications sheet.

Specification	Value
Color	Infrared (IR)
Nominal Wavelength	780 nm
Power LED Output (Min)	200 mW
Power LED Output (Typical)	300 mW
Test Current for Typical LED Power	800 mA
Maximum Current (CW)	800 mA
Forward Voltage	2.0 V
Bandwidth (FWHM)	28 nm
Viewing Angle	20°
Typical Lifetime	>10,000 h

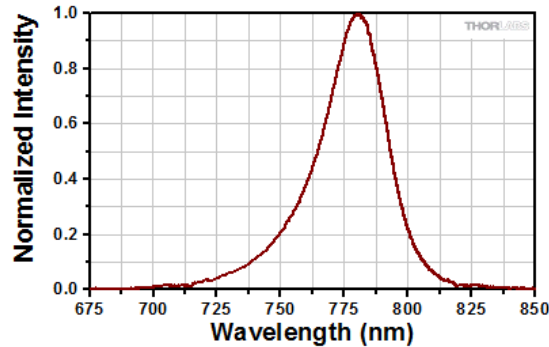


Figure 6: Thorlabs 780L3 LED normalized intensity versus wavelength plot.

This wavelength was chosen due to the greater depth of imaging which can be acquired with longer wavelength light sources (Kobalt et al., 2009). Using a shorter wavelength of light would provide a higher resolution due to the shorter steps required for imaging. This is the case because the step size is dependent on the wavelength. This would result in a greater number of images and bulkier data files. Since this project focused on imaging multiple surfaces and internal structures, high imaging depth was required without greatly sacrificing accuracy of the recorded images. Thus a middle ground needed to be reached where the selected wavelength

needed to be short to ensure high resolution yet long enough for proper imaging depth, which resulted in the aforementioned wavelength of 780nm.

### 3.1.2 Piezo

To ensure that both surfaces could be imaged, a travel distance which was greater than the thickness of the sample was needed. Available to the group were a few different nano-positioners which could perform steps that were small and accurate enough to use OCT, yet provide great enough travel to ensure thickness data would be gathered. The primary types of positioners available for the project consisted of piezoelectric microscope objective positioners and single axis nano-positioners. The piezoelectric positioners were made by Physik Instrumente and had total travel of 18 and 200 microns. The advantages of the piezoelectrics include positioning resolution of less than one nanometer and high response for fast settling and scanning. The single axis nano-positioners are manufactured by Newport and have a minimum incremental step of 0.1 microns and a total travel of 50mm.

The positioner that was selected for the optical coherence tomography setup was the PI piezoelectric objective positioner. The group was able to get a loaner piezo from PI to carry out experimentation with a total travel distance of 400 microns. The extended travel ensured that any sample imaging would not be limited by the travel or accuracy of the positioner.

### 3.1.3 Objective

For this experiment an objective with an interferometer was needed to ensure the optical coherence tomography functioned properly. Available for the project were three interferometric objectives made by Leica. Of them, two were Michelson interferometers with magnifications of 5x and 10x. These lenses have tunable object and reference mirrors which are used for changing how the interference patterns appear on the sample surfaces. The third objective had consisted of a Mirau interferometer with a magnification of 20x. The Mirau lens has fixed mirrors with a very small path difference allowing for greater accuracy in interferometric measurements. All of the lenses are equipped with an object beam limiter which allows for beam ratio modification.

With all the properties of the interferometric parts of the objectives known, the next aspect that needed to be considered was the actual properties of the lenses and how they affected the imaging of the system. The most important factors to consider for OCT experimentation are the magnification, focal length, numerical aperture, and working distance which can be seen in Figure 7 and are described in the following Section.

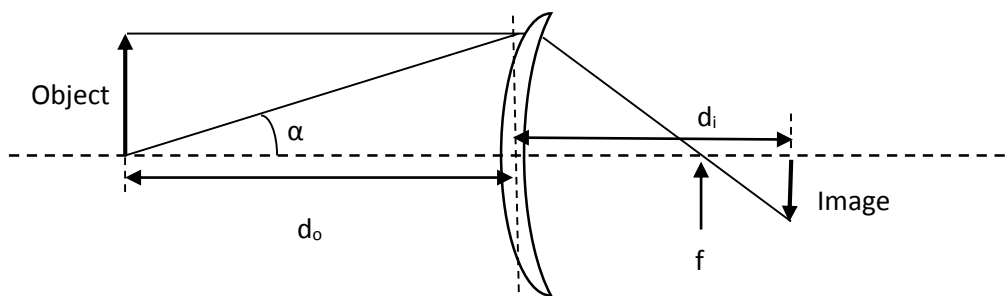


Figure 7: Geometric optics for a simple lens.

Magnification of the objective is the ratio of the distance of the image to the lens to the distance of the sample to the lens give as

$$M = -\frac{d_i}{d_o},$$

where  $d_i$  is the image distance and  $d_o$  is the object distance. Focal length can be represented by the Lens Equation and is the location at which the image is focused on the camera sensor. Focal length is important because it is used to determine other optical properties of the lens and is defined as

$$\frac{1}{f} = \frac{1}{d_i} + \frac{1}{d_o}.$$

Numerical aperture represents the range of angles at which light can be accepted by an objective and can be represented by the index of refraction of the viewing medium  $n$  multiplied by the sine of the acceptance angle of the lens,

$$NA = n * \sin(\alpha).$$

Working distance is defined as the distance from the end of the objective to the surface of the sample at which point the sample is in focus. Working distance is extremely important for OCT when imaging multiple surfaces primarily due to the fact that if the working distance is too small, the front of the objective will come into contact with the sample before imaging internal surfaces.

$$WD = \frac{f}{(1 + \frac{1}{M})}$$

Table 2 shows corresponding values for each lens available for the OCT setup.

*Table 2: Key lens properties for use in OCT for each available lens.*

Lenses	Magnification	Working distance (mm)	Numerical Aperture
Leica HCX PL FLUOTAR 5x/0.15	5x	13.70	0.15
Leica HCX PL FLUOTAR 10x/0.30	10x	11.00	0.30
Leica HCX PL FLUOTAR 20x/0.50	20x	1.15	0.50

Based on the optical properties of the lenses, the Leica HCX PL FLUOTAR 5x/0.15 was the lens that was selected for the experimentation. Even though the magnification was not as large as what was available from other lenses, the higher working distance is the primary reason for this selection. The lenses with the lower working distances would provide images with greater detail due to their higher magnifications but there would not be enough distance from the end of the objective to the sample to ensure a second surface would be imaged. The 5x magnification also provided the largest imaging area allowing for greater portions of the sample to be imaged simultaneously. This greater imaging area also provided more structures of the samples to be observed in single runs of the OCT.

### 3.1.4 Camera

With the light source, positioner, and objective decided upon, the camera selection could be optimized to ensure the best results. The available cameras included a Pike F145-B and a Pike F100-B. The primary difference between these cameras are the pixel resolution of the camera with the PIKE F100B having being a 1 mega pixel camera and the Pike F145-B being a 1.4 mega pixel camera. Other than the pixel resolution difference, each camera has a different spectral

response meaning they are more effective at certain wavelengths which can be seen in Figures 8 and 9.

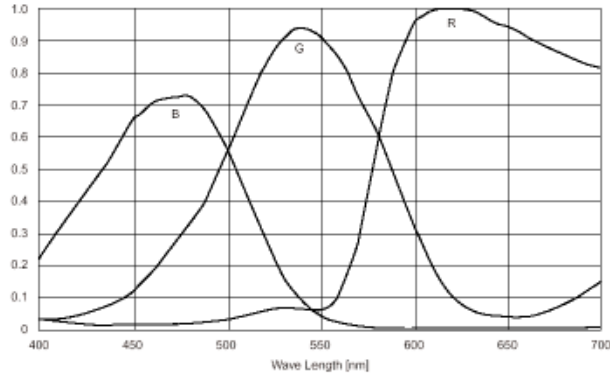


Figure 8: Spectral response of the Pike F145-B for overall and individual color relative to wavelength.

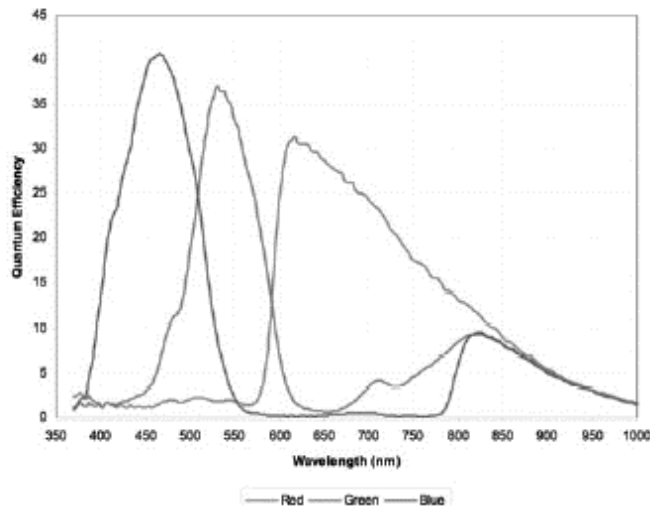


Figure 9: Spectral response of the Pike F100-B for individual color relative to wavelength.

Since the optimal wavelength for maximum imaging depth that was selected for the OCT setup was 780nm, the camera needed to operate well at that wavelength. The Pike F145B had a higher efficiency while imaging high wavelengths when compared to the F100-B which has roughly an efficiency of 15% at 780nm. Because the Pike F145-B had the higher efficiency for

the wavelength used in the setup it would provide higher quality images and therefore the best choice for the setup.

## 3.2 Procedure

With the setup completed and optimized for obtaining thickness measurements of the sample, imaging could now take place. The following section describes the steps that were taken to prepare the OCT setup for experimentation and then how it was actually used to acquire images. Also included is the description of how the obtained images were processed so that information about the sample such as thickness and internal structures could be gathered.

### 3.2.1 Sample Preparation

To obtain significant data, a sample must first be obtained to work with. There were two main requirements for the sample: is it thin enough, and do the optical properties of the sample correlate with the system (i.e. will interference happen at the surfaces). For the first requirement a micrometer was used to measure the thickness value of the sample. The second requirement was fulfilled through online research of the specimen. For samples that did not have optical properties that could be looked up, the sample was imaged manually with the OCT setup to determine if two interference patterns were visible. Roscolux color swatches were used for validation which had both of the needed parameters included their specification sheet. With the sample preparation completed the next step was to start the image acquisition.

### 3.2.2 Image Acquisition

The image acquisition software used was LaserView which is an in-lab developed software from the CHSLT labs (Harrington et al., 2010). This software takes all the images and saves them as a video file which can then be used for the processing. However, the control of this software is done by both Labview and the camera used.

The Labview program works by sending a voltage to the piezo, this causes it to move to a specific location. To get the desired step increment, voltage was increased, essentially stepping the voltage up which in turn increases the piezo distance. At the same time, the Labview program sent a trigger signal to the camera. This trigger was in the form of a 5 Volt square wave. Then the camera in turn sent a signal to Laserview and the image was recorded. Then the voltage was stepped again and the process was repeated until the desired travel was achieved.

### 3.2.3 Image Processing

The image processing for the project was completed in Matlab. The key steps done consisted of transposing the acquired image matrix, recording a single pixel intensity values across the scanned media, making an envelope of the data through calculation of the Hilbert transform of the data, obtaining the peak values from the envelopes, storing these values in other matrices, calculating the intensity modulation for the A-Scan and B-Scan, and plotting the acquired data into a three-dimensional image.

## 4.0 Validation

With the setup and procedure for the optical coherence tomography experiment completed and data acquired, validation of the system was needed to prove that it works effectively and that it is accurate. To test the validity the OCT system, inorganic samples with known characteristics were imaged so that the measured thickness could then be compared to the known values. This would give a baseline accuracy of the system that could be applied to samples of unknown or varying thickness such as biological samples.

The samples used for validation of the OCT system were taken from the Roscolux color swatchbook by Rosco. These samples are a combination of roughly 65% co-extruded polycarbonate plastic combined with dyed polyester. These samples act as filters, absorbing specific wavelengths and transmitting others depending on the color of the swatch. For the experimentation it was vital to select sample swatches that would have low absorption of the incident radiation so enough could be transmitted through the entirety of the sample. Also with the great variation of swatches available, the effectiveness of the developed system could be evaluated based on varying sample optical properties. The sample colors that were selected based on their ability to transmit light at 780nm included Scarlet, Tough Plusgreen, Gaslight Green, and Cerulean Blue.

When looking at the spectral distribution of the 780nm light source used for experimentation it was apparent that the wavelengths which are produced by the diode range from 715 to 820 nm with the highest intensity at 780nm. The given transmission graphs from Rosco stopped at 750 nm but the selected samples showed high percent transmission for at least a portion of the diode's wavelength range as seen in Figure 10.

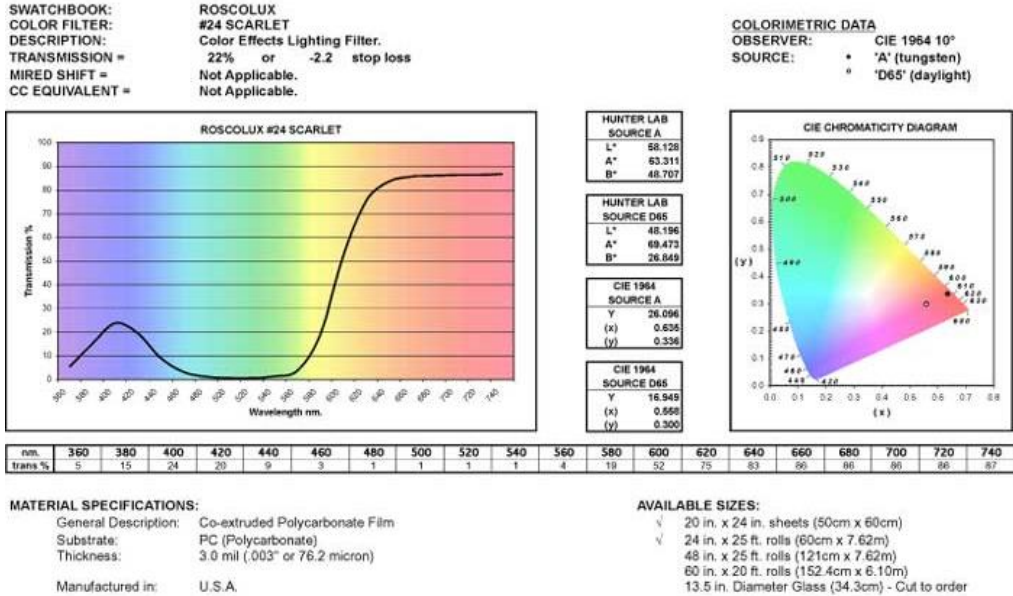


Figure 10 Roscolux scarlet color filter technical data sheet used.

The scarlet sample was chosen because it displayed a relatively constant transmission of 86% for the lower range of the light source but the transmission for the higher part of the range was not provided. From the provided technical data sheet, the listed thickness of this color swatch was 0.003 inches or 76.2 microns. The swatch was then physically measured using calipers and a thickness of  $0.0030 \pm 0.0005$  inches was recorded. With the actual thickness known, the swatch was then imaged using the OCT setup. The images gathered were then processed using Matlab to see if multiple surfaces were detected. A single pixel was selected, processed, thus resulting in Figure 11, which depicts the change in light intensity as the swatch was imaged.

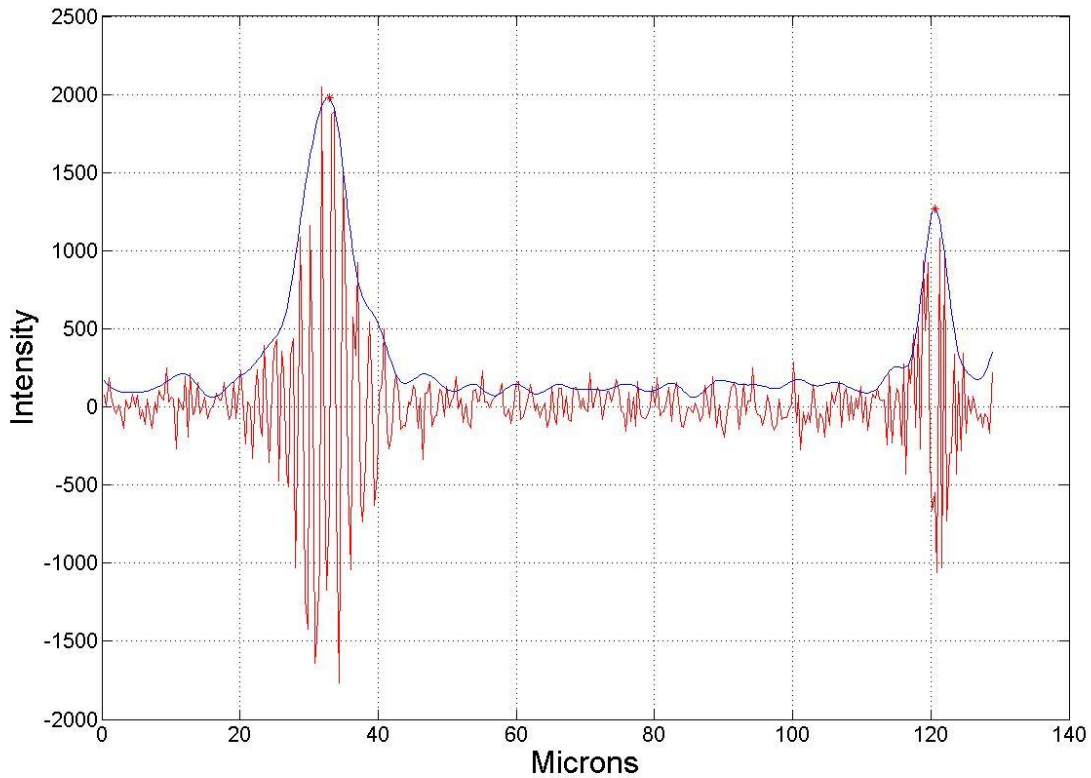
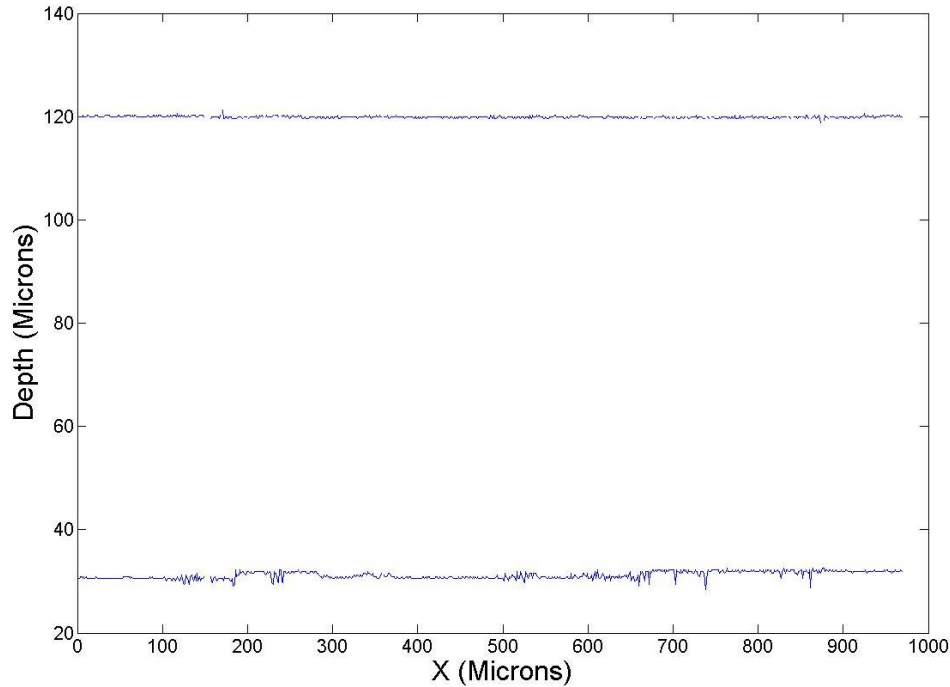


Figure 11: Recorded interference pattern for 2 surfaces of a Scarlet Roscolux color swatch.

From these data it is apparent that two areas of interference were detected. From the images gathered, 750 pixels were selected and from them the average distance between maximum interference intensities were calculated. The first interference pattern occurred on average after 18.23 microns with a standard deviation of 0.11 microns. The second detected interference pattern was detected on average after 90.46 microns of travel with a standard deviation of 0.16 microns as observed below in Figure 12.



*Figure 12: Measured Scarlet Roscolux color swatch thickness map plot showing both surfaces.*

The results indicated an average distance of  $72.22 \pm 0.19$  microns separating the two interference patterns. For this sample the average thickness calculated from the OCT measurements was 5.36% different than the known thickness.

With the average thickness of the sample determined, the system needed to be tested to verify if internal structures could be imaged. To do this an intensity modulation was performed on a cross section of the image stack. As mentioned in the background, cross sections of this type are known as B-Scans and represent the reflections that are occurring as the sample is imaged. For samples with internal structures, light will interact with any non-uniformity and a reflection will occur. Because of this a B-Scan will display any internal structure in which a reflection takes place. Unfortunately the Roscolux color swatches are uniform and contain no internal structures so when a B-Scan is performed no reflections will be displayed other than the initial

and final surfaces. To verify this is the case, a B-Scan was performed and is displayed below in Figure 13. As expected there are no internal reflections between the surfaces.

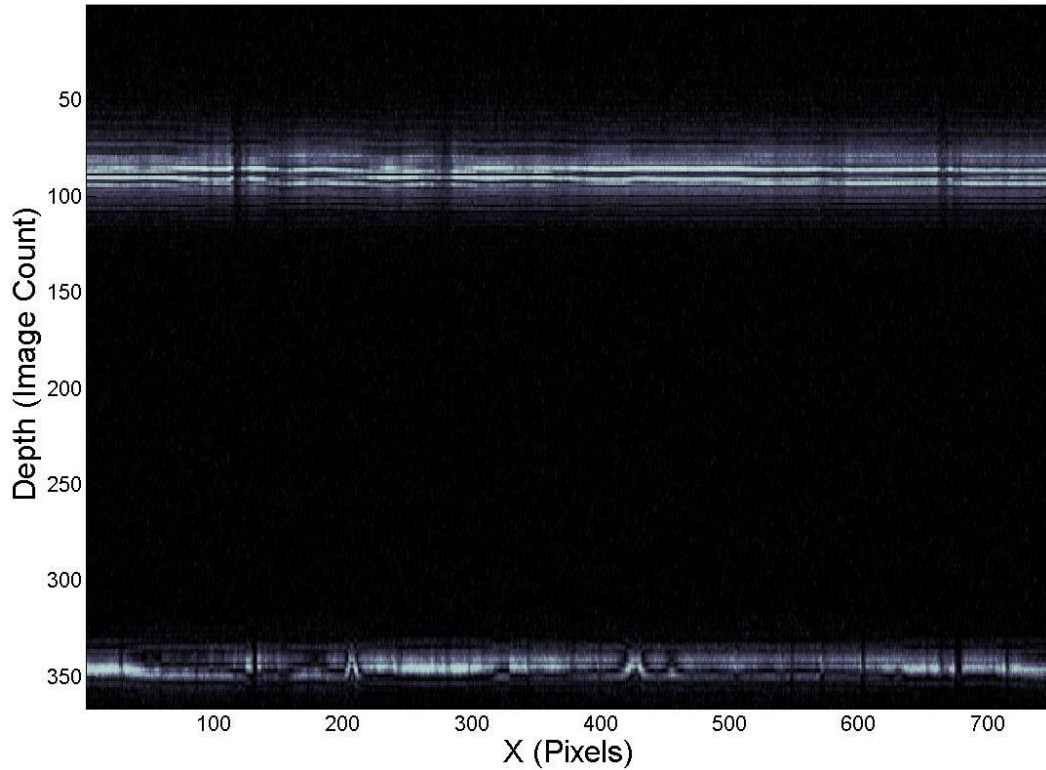
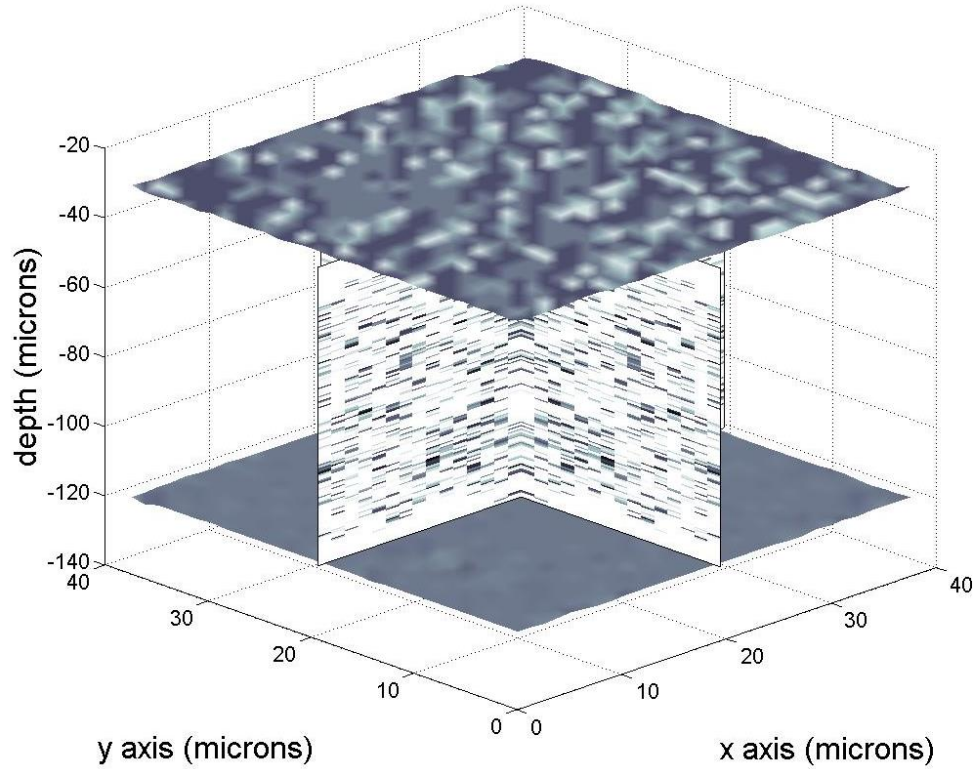


Figure 13: Measured B-Scan of a Scarlet Roscolux color swatch.

By storing the intensity peaks' locations from the individual pixels in a matrix, a three dimensional figure can be plotted to show the topography of the sample. When plotted along with the B-Scans of the sample, a three dimensional figure is generated that contains information on both the surfaces and any internal structures as seen in Figure 14. This was done for the validation swatches to show what the completed figure looked like and how information can be gained from it.

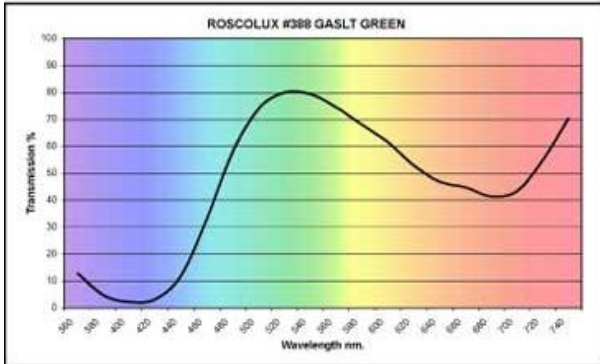


*Figure 14: Measured 3-dimensional figure of a Scarlet Roscolux color swatch of both surfaces and its internal structures.*

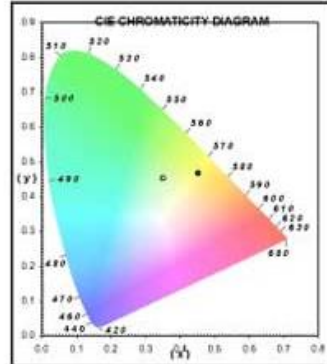
This validation procedure was repeated using other color swatch samples to show how different optical properties such as color, transmission, absorption and reflection effect the accuracy of the system. For the Gaslight Green color swatch the percent transmission showed an increasing trend for the 700-740nm range of the spectrum as seen in Figure 15.

SWATCHBOOK: ROSCOLUX  
 COLOR FILTER: #388 GASLT GREEN  
 DESCRIPTION: Color Effects Lighting Filter.  
 TRANSMISSION = 76% or -0.4 stop loss  
 MIREL SHIFT = Not Applicable.  
 CC EQUIVALENT = Not Applicable.

COLORIMETRIC DATA  
 OBSERVER: CIE 1964 10°  
 SOURCE: \* 'A' (tungsten)  
 ° 'D65' (daylight)



HUNTER LAB SOURCE A	
L*	85.682
A*	-18.186
B*	37.927
HUNTER LAB SOURCE D65	
L*	86.322
A*	-29.204
B*	46.684
CIE 1984 SOURCE A	
Y	67.373
(x)	0.462
(y)	0.468
CIE 1984 SOURCE D65	
Y	68.633
(x)	0.381
(y)	0.463



nm.	360	380	400	420	440	460	480	500	520	540	560	580	600	620	640	660	680	700	720	740
trans %	13	5	2	3	12	33	58	74	80	79	74	68	62	53	47	45	42	44	55	70

**MATERIAL SPECIFICATIONS:**  
 General Description: Co-extruded Polycarbonate Film  
 Substrate: PC (Polycarbonate)  
 Thickness: 3.0 mil (.003" or 76.2 micron)  
 Manufactured in: U.S.A.

**AVAILABLE SIZES:**  
 ✓ 20 in. x 24 in. sheets (50cm x 60cm)  
 ✓ 24 in. x 25 ft. rolls (60cm x 7.62m)  
 48 in. x 25 ft. rolls (121cm x 7.62m)  
 60 in. x 20 ft. rolls (152.4cm x 6.10m)  
 13.5 in. Diameter Glass (34.3cm) - Cut to order

Copyright 2001, Rosco Laboratories Inc.  
 All Rights Reserved

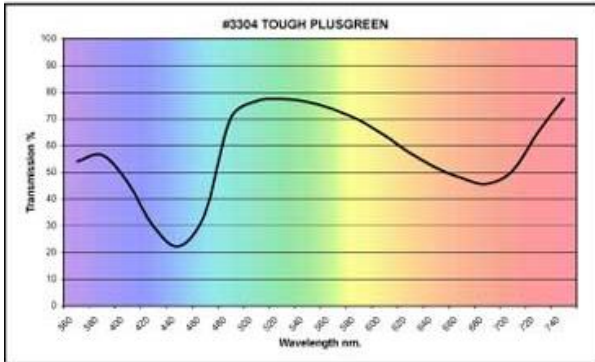
Figure 15: Roscolux Gaslight Green color filter technical data sheet used.

Similar to Scarlet, 750 pixels were selected and the average thickness was calculated to be  $71.13 \pm 0.23$  microns. The measured and specified thickness of the Gaslight Green swatch was 76.2 microns giving a percent difference of 6.87%.

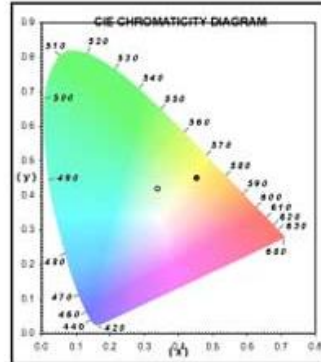
Tough Plusgreen showed a similar transmission spectrum as Gaslight Green but the reason for imaging this sample was because it had a thickness of 0.002 inches or 50 microns from Figure 16.

SWATCHBOOK: ROSCOLUX  
 COLOR FILTER: #3304 TOUGH PLUSGREEN  
 DESCRIPTION: Color Balancing Lighting Filter. Adds Green.  
 TRANSMISSION = 76% or -0.4 stop loss  
 MIREID SHIFT = Not Applicable.  
 CC EQUIVALENT = cc 30 Green

COLORIMETRIC DATA  
 OBSERVER: CIE 1964 10°  
 SOURCE: \* 'A' (tungsten)  
 ° 'D65' (daylight)



HUNTER LAB SOURCE A	
L*	86.220
A*	-14.401
B*	27.116
HUNTER LAB SOURCE D65	
L*	86.819
A*	-23.066
B*	33.109
CIE 1964 SOURCE A	
Y	66.420
(x)	0.453
(y)	0.451
CIE 1964 SOURCE D65	
Y	69.638
(x)	0.339
(y)	0.419



nm.	360	380	400	420	440	460	480	500	520	540	560	580	600	620	640	660	680	700	720	740
Trans %	54	56	46	30	22	34	70	77	77	76	74	70	64	57	52	48	46	51	65	78

MATERIAL SPECIFICATIONS:  
 General Description: Deep-dyed polyester film  
 Substrate: PET (Polyethylene Terephthalate)  
 Thickness: 2.0 mil (.002" or 50 micron)  
 Manufactured in: U.S.A.

AVAILABLE SIZES:  
 ✓ 20 in. x 24 in. sheets (50cm x 60cm)  
 ✓ 24 in. x 25 ft. rolls (60cm x 7.62m)  
 ✓ 48 in. x 25 ft. rolls (121cm x 7.62m)  
 60 in. x 20 ft. rolls (152.4cm x 6.10m)  
 13.5 in. Diameter Glass (34.3cm) - Cut to order

Copyright 2001, Rosco Laboratories Inc.  
 All Rights Reserved.

Figure 16: Roscolux Tough Plusgreen color filter technical data sheet used.

To investigate if the setup performed differently when varying sample thickness while optical properties remained similar, the results of characterizing both of these samples were compared. By following the same procedure used for measuring the other swatches, a thickness of  $49.0 \pm 0.42$  microns was measured from the OCT setup. This value was 1.95% different than the measured and specified thickness. This sample had a much lower percent difference than the larger samples but a standard deviation that was roughly twice as large. From this, the OCT setup appears to be more accurate when imaging thinner samples yet less precise when compared to samples of greater thickness.

To determine the performance of the system when imaging a sample having low transmission for the 780 nm light source, the Cerulean Blue swatch was imaged. This sample has

a reported transmission of 0% for the lower part of the light source spectrum of 700-740nm. Like in the other samples, the transmission for wavelengths past 740 were unknown so for this sample there was some chance that a portion of the light would be transmitted.

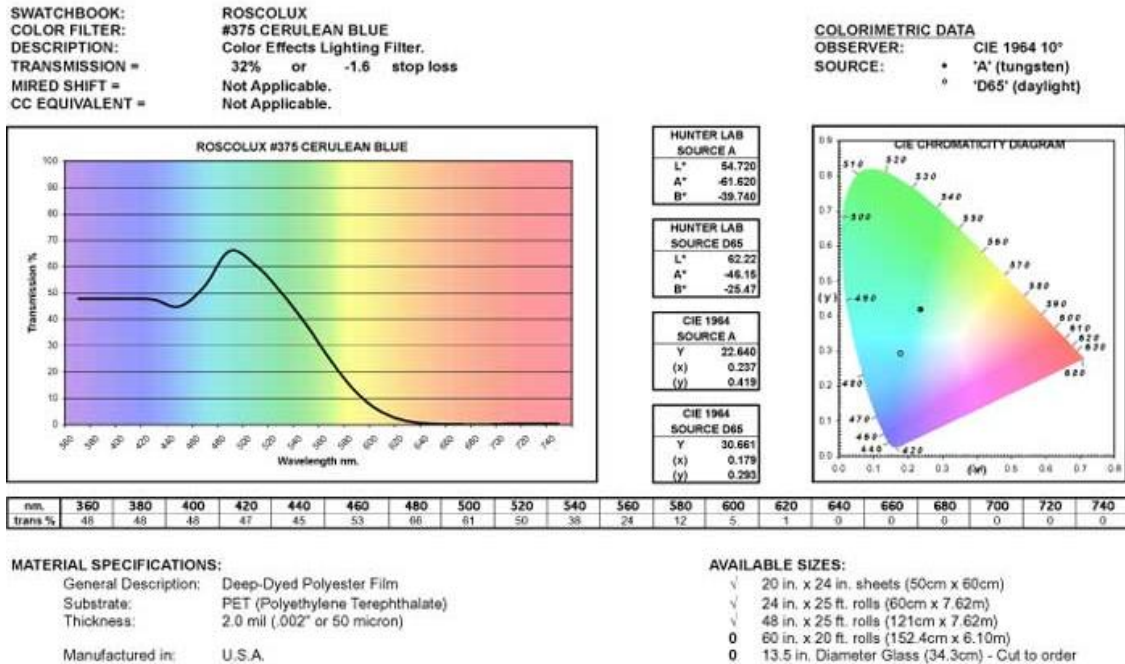


Figure 17: Roscolux Cerulean Blue color filter technical data sheet used.

However as expected, this was not the case. When using the 780nm light source only a first surface was detected and a second peak was not visible. To determine if a second surface could actually be imaged, the light source was replaced with a 530nm source which had a 50% transmission, just for comparison. Using the 530nm light source, a second intensity peak was detected but at a significantly lower intensity when compared to the first peak which is shown in Figure 18.

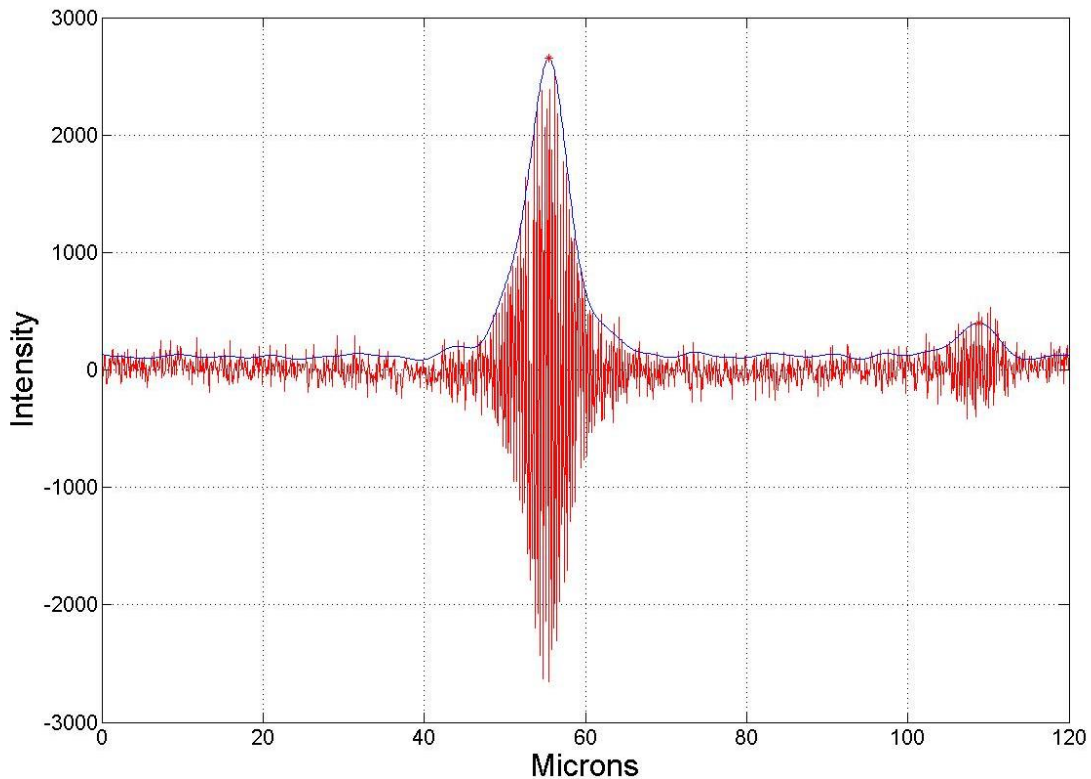


Figure 18: Measured intensity distribution of a Cerulean Blue Roscolux color swatch using the 530nm LED.

This is an important finding because it shows that even when there is low transmission the system is still able to detect a second peak. It should also be noted that a second peak was only detected in a fraction of the total pixels. This was most likely due to the camera's ability to operate at the 530nm wavelength was not as optimal as when using the 780nm source. Even though thickness values were not attainable for all pixels, there was a sufficiently large enough quantity so that an average thickness could be calculated. The measured and specified thickness for this sample was 0.002 inches or 50 microns and the average thickness measured by the OCT setup was 48.6 microns. This results in a 2.75% difference from the known thickness. Even though the percent difference for this color swatch was lower than the other samples, it should be

noted that the standard deviation for this sample was  $\pm 8.2$  microns. This variation can most likely be attributed to the relatively low sensitivity of the camera to detect a 530 nm light source.

## 5.0 Biological Samples

Validation of the OCT setup provided a baseline precision of the system for uniform samples which could then be applied to non-uniform specimens such as biological samples. To do this, biological samples needed to be imaged. This part of the experimentation proved to be difficult due to the various internal structures and optical properties present in non-uniform samples such as these. The reason that obtaining useable images from our OCT setup was more difficult for biological samples was caused by the light propagating through the sample being absorbed or scattered. In the case of the uniform samples tested for system validation, once light entered the sample it could travel unhindered towards the second surface. This occurred because the Roscolux color swatches are a combination of co-extruded polycarbonate plastic and dyed polyester at a constant proportion throughout. With no sudden index changes other than the first and second surfaces, no other reflections would occur at locations other than those two points. However when imaging the biological samples, at every cell boundary there is an area where light could be scattered. The more cells that the light passes through, the more scattering occurs and thus less light is allowed to propagate through the sample. This led to many cases where not enough light was able to travel through the sample to the second surface and then back to the camera. Without a well-defined second interference pattern, it becomes increasingly difficult to provide an accurate thickness of the specimen.

With the primary obstacle in the way of obtaining good images being scattering caused by internal structures, focus was shifted towards how different internal structures stop light from propagating. To do this, several different specimens of varying cell sizes were imaged so that conclusions could be made and also so a strategy for obtaining thickness of biological samples could be devised. The biological samples imaged included internal and external epidermal onion tissue, garlic tissue, celery stalk, celery leaves, embryonic membrane of a chicken egg, and leaves from various plants.

For biological samples the 780nm was selected for imaging due to the greater travel potential the longer wavelength offered. Unfortunately, not all samples displayed a secondary peak after the primary surface. This was most likely due to their ability to transmit light at 780nm was too low to allow for a decent light propagation distance. As observed in the case of the Cerulean Blue color swatch, by switching the light source it was possible to attain improved imaging, but this was not a feasible option when attempting to develop a single OCT setup which could image various samples

However, two samples did provide good secondary peaks when imaged using the 780nm source. These samples, internal epidermal onion tissue and celery stalk, will be described in detail in the next Sections.

## 5.1 Internal Epidermal Onion Tissue

The onion sample that was imaged was the internal epidermal onion tissue. This part of the onion is the thin membrane which is located between the two larger layers in the bulb of the onion. For the 780nm wavelength, this type of onion skin has a transmission of roughly 40%

(Stair, 1935). Even though this percent transmission is roughly half than the transmission of the validation samples, in some areas multiple surfaces were detected. Figure 19 shows an A-Scan of the onion sample and in it two distinct surfaces are visible.

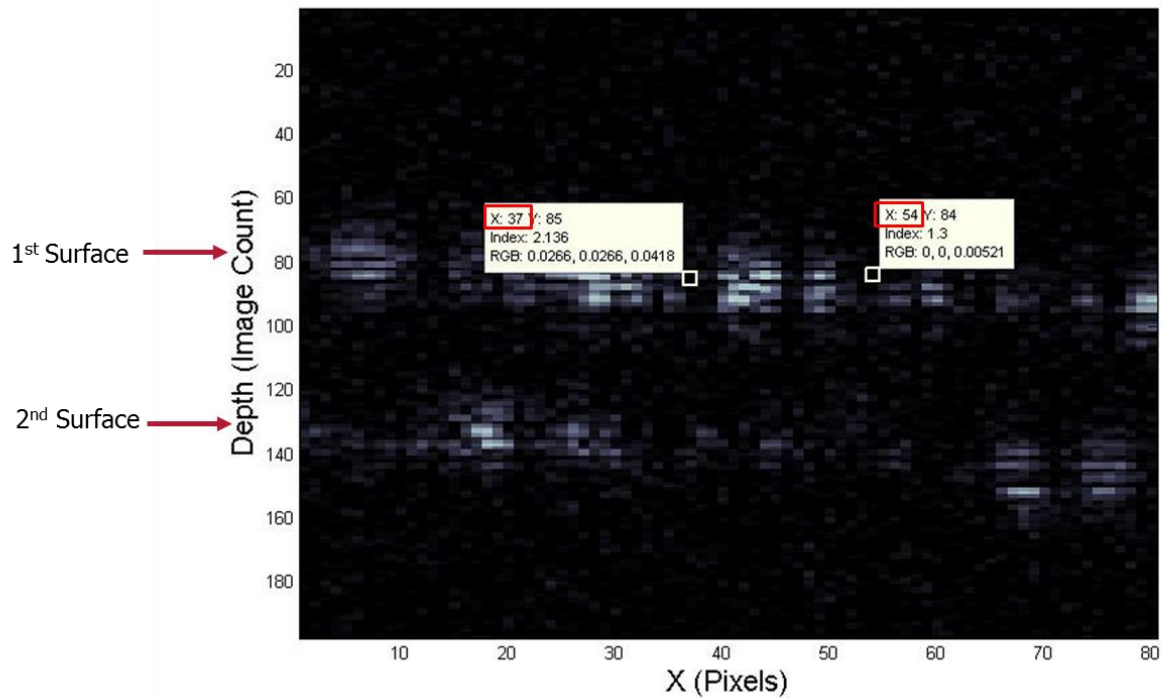


Figure 19: An A-Scan of an inner epidermal layer of an onion sample.

To ensure that the two reflection areas are indeed the first and secondary surfaces, the onion sample was mechanically measured using calipers. This method of measurement for biological samples is not very precise due to the stresses that are induced on the sample when measured using the calipers. Deformations along with cellular structure damage could lead to error in this type of thickness measurement but it does give a ballpark idea on how thick the sample is. The measured value obtained from the calipers was 26 microns. Even though a thickness measurement could not be obtained from every pixel, there were a significant amount

of quality pixels to select from and thus an average thickness of the onion sample could be calculated from the OCT images. That calculated thickness value was  $49.9 \pm 3.28$  images thick which is visible in the A-Scan (Figure 19). When converted into microns the thickness is  $19.5 \pm 1.3$  microns. This value gives a 28.6% difference than the thickness which was measured using the calipers. Like previously mentioned, the caliper measurement may have caused a deformation in the sample to result in erroneous thickness measurements. When researching typical onion epidermal cell diameters it is noted that cell diameter varies significantly depending on the age and type of the onion. Since the age could not be verified in our samples, specified thickness was not a precise way to validate this specific thickness measurement.

Other than thickness, individual cells and their cell boundaries were visible in the A-Scans. When looking at the A-Scan, there are distinct dark areas that are located on both the top and bottom surfaces. In the actual OCT images cell walls and boundaries between cells did not produce interference patterns whereas the cell surfaces did. To verify if these dark areas were indeed cell boundaries, a single image from the OCT stack was used to count the number of pixels that made up the width of each cell. This was repeated for several cell widths resulting in an average measured width of  $24.0 \pm 2.5$  microns. The distances displayed in the A-Scan matched this measured cell width thus proving that individual cells were able to be distinguished from one another when displayed in the A-scan. Also visible in the A-scan was the internal cell boundaries. When looking at the individual cells in the surfaces distinct boundaries can be made out inside of the sample. For some of the cells there appears to be a halo of lighter areas that gradually faded, which can be observed in Figure 20.

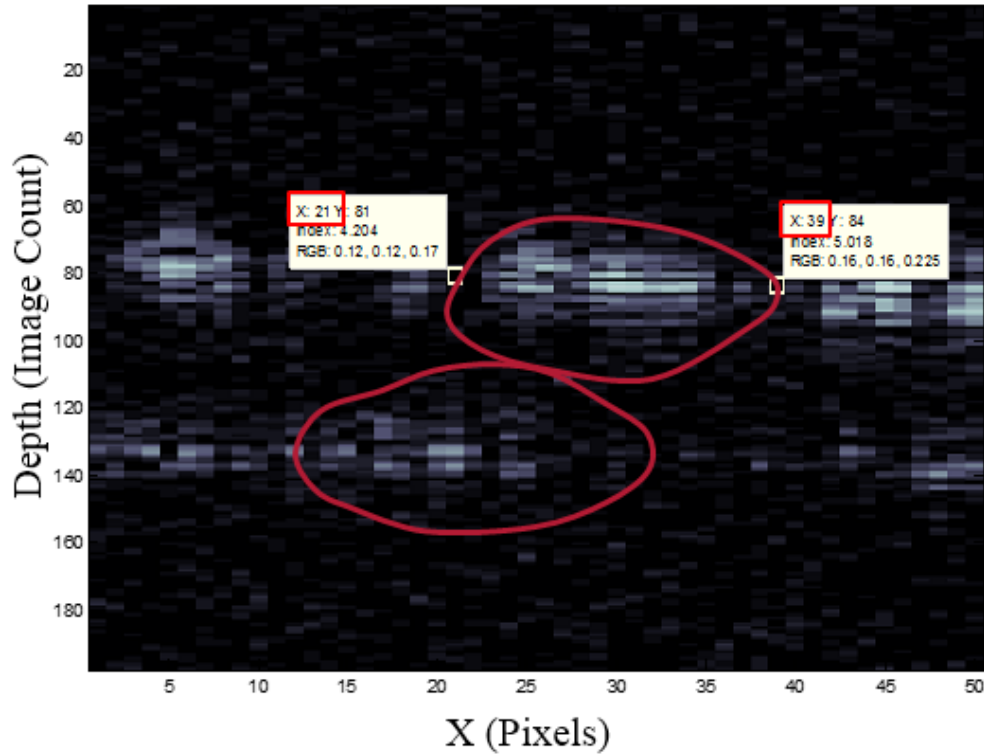
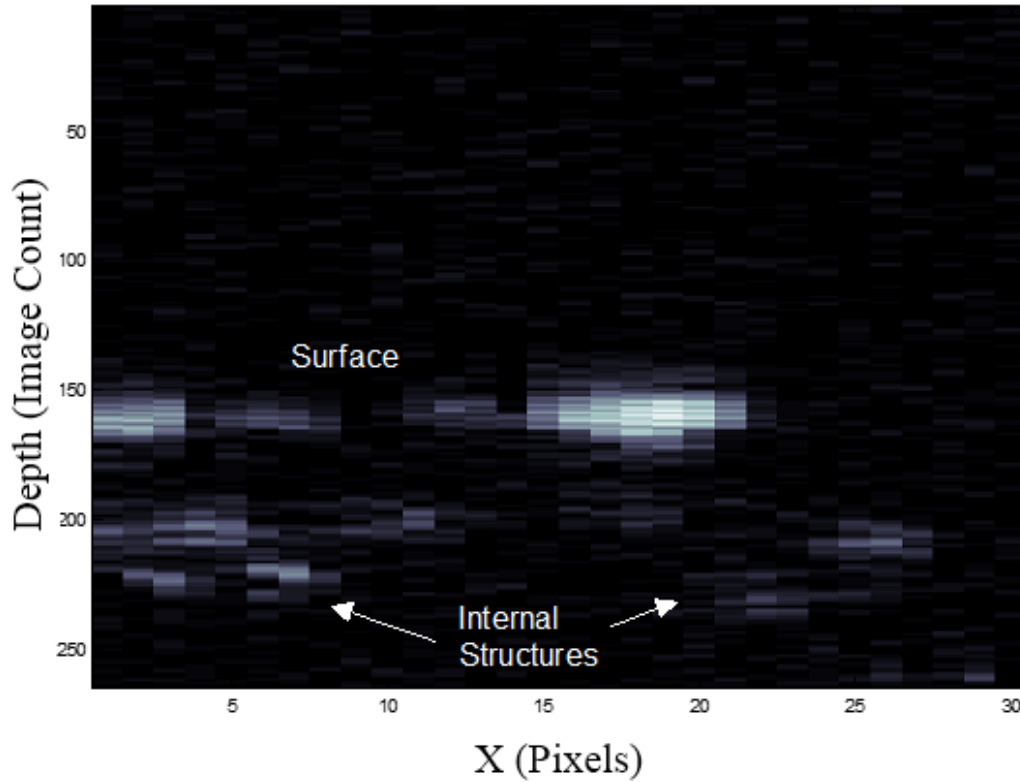


Figure 20: A-Scan of an inner epidermal layer of an onion sample depicting cell boundaries.

Two of these boundaries have been outlined in the A-Scan to help display the individual cells. This finding is valuable for the experimentation because it shows that not only thickness of biological samples can be obtained but individual cells can be differentiated from one another.

## 5.2 Celery Stalk

With thickness of a biological sample shown, the next test for the OCT system was to determine the imaging depth that could be obtained for a biological sample. Before imaging, it was expected that imaging depth would be limited due to the scattering that occurs at cell boundaries. However, when imaging the celery stalk, an imaging depth of nearly 160 microns was attained.



*Figure 21: An A-Scan of a celery stalk sample with internal structures visible.*

From the A-Scan shown in Figure 21, the surface was imaged and then various internal structures were also visible. This is interesting because celery stalk has larger and more rigid cells on the surface and then smaller cells internally. In the A-Scan the surface was successfully imaged and then even though they varied, the smaller internal cells were also visible. Celery stalks also contain large water transporting structures throughout, and it is possible that the two larger internal structures that are visible could be seen in Figure 21.

## 6.0 Conclusions

The Spatial Optical Coherence Tomography system that was developed specifically from obtaining thickness of samples both biological and synthetic works within an acceptable range of error. The sampling of non-biological samples which contain uniform compositions provide clear and accurate data that requires almost no noise removal. This is due to the uniformity of the sample both on the surface and internally. On the other hand, biological samples with varying surfaces and internal structures that disrupt light propagation throughout the sample make imaging significantly more difficult when attempting to obtain meaningful data. The increased scattering causes an increase in the number of erroneous pixels and because of that, the resulting three dimensional imaging is not very effective. However, through using the A/B-Scans of the biological samples, which display the intensity modulations returning to the camera, both thickness and internal structures were visible. Unfortunately because the samples were still not particularly uniform, only specific areas of the sample provided accurate data. Due to this, fine tuning of the setup is key, with large travel ranges, optimal wavelength, and a large working distance from the objective being necessary to obtain accurate and reliable results from biological samples.

## 7.0 Future Work

Some of the improvements that can be done are related to the recording of the images. Even though the triggering goes to the camera, it does not start recording immediately, therefore some frames are missing. By correcting this, more precise data can be obtained.

Other improvements on the system can be made, such as fully automating both the acquisition and processing of the data. These processes, especially the later, can take a substantial amount of time. By automating these aspects even more, either by being able to obtain all the required parameters directly from the data and not having to input them manually would save time and increase productivity. Different levels of improvement can be made with the use of different higher precision equipment, such as achieving motions that produce 90 degrees phase changes.

## References

- Bennett, B T, Bewersdorf, J, Gould, T J, Hess, S T, Juette, M F, Lessard, M D, Nagpure, B S, "Three-dimensional sub-100 nm resolution fluorescence microscopy of thick samples," *Nature Methods*, 5(6), 527, 2008.
- Boeglin, W, "Michelson Interferometer," *Florida International University*. Florida International University, <[http://wanda.fiu.edu/teaching/courses/Modern\\_lab\\_manual/michelson.html](http://wanda.fiu.edu/teaching/courses/Modern_lab_manual/michelson.html)>, Last Accessed, October 2014.
- Harrington E, Dobrev I, Bapat N, Flores J, Furlong C, Rosowski J, Cheng J, Scarpino C, and Ravicz M, "Development of an optoelectronic holographic platform for otolaryngology applications," *Interferometry XV: Applications 7791*, 2010.
- Huang D, "OCT Terminology – Demystified," *Ophthalmology Management*, Issue: April, 2009.
- Huang D, Swanson EA, Lin CP, Schuman JS, Stinson WG, Chang W *et al.*, "Optical Coherence Tomography," *Science*, 254(5035): 1178–1181, 1991.
- Kobalt D, Durst M, Nishimura N, Wong A, Schaffer C B, and Xu C, "Deep tissue multiphoton microscopy using longer wavelength excitation," *Opt. Exp.*, 17: 13354-13364, 2009.
- Larkin K G, "Efficient nonlinear algorithm for envelope detection in white light interferometry," *J. Opt. Soc. Am. A*, 13(4): 832 –843, 1996.
- Liu B, Vercollone C, and Brezinski M E, "Towards Improved Collagen Assessment: Polarization-Sensitive Optical Coherence Tomography with Tailored Reference Arm Polarization," *Int. J. Biomed. Img.*, 892680. doi:10.1155/2012/892680, 2012.
- Mahadevan S *et al.*, "An Inexpensive Field-Widened Monolithic Michelson Interferometer for Precision Radial Velocity Measurements," *Publications of the Astronomical Society of the Pacific*, DOI:10.1086/592197, 2008.
- Quimby R, *Photonics and Lasers: An Introduction*, Hoboken, NJ: John Wiley and Sons, Inc., 2006.

Radhakrishnan S, Goldsmith J, Huang D, *et al.*, "Comparison of Optical Coherence Tomography and Ultrasound Biomicroscopy for Detection of Narrow Anterior Chamber Angles," *Arch Ophthalmol.*, 123(8):1053-1059. doi:10.1001/archophth.123.8.1053, 2005.

Schmitt J M, "Optical coherence tomography (OCT): a review," *IEEE Journal of Selected Topics in Quantum Electronics* **5** (4): 1205, 1991.

Sutter R and Davidson M, "Interference between Parallel Light Waves," *Molecular Expressions*, National High Magnetic Field Laboratory,  
<http://micro.magnet.fsu.edu/primer/java/interference/waveinteractions2/index.html>,  
Last Accessed October 2014.

Stair R and Coblenz W W, "Infrared absorption spectra of plant and animal tissue and of various other substances," *J. Res. Nat. Bur. Stand*, **15**, 295-316, 1935.

# Appendix

## Single Pixel Code

```
clear; clc; close all;
tic

% Opening the images and isolates one pixel
x=155; y=519;
num_images=371;
total_microns=128.9;

Vid=openLVVid('400micron_piezo_test_toughplusgreen_onestep.lvvid'); % In
Essential Files
Image_stack=zeros(1,num_images);

Frame_num=zeros(Vid.imageHeight,Vid.imageWidth);

for i=1:num_images
    Pixel = getLVVidPixel( Vid,i,x,y);
    Image_stack(1,i)=Pixel;
end

%Plot of Intensity Variation and Envelope Generation

% Measure the intensity axially along a pixel
Intensity=(Image_stack(1,:));
z=(total_microns/num_images):(total_microns/num_images):total_microns;
A=Intensity(:);
s=detrend(A);% Make the mean values of the intensity modulation zero to aid
in analysis

% Filtering the acquired data using a low pass filter
dz=(total_microns/num_images);
filter_cutoff=(1/(2*dz))-0.01;
sF=my_filter(s, dz, filter_cutoff); %In Essential MatLab Files

% Plot of intensity variation for 1 pixel
plot(z,sF,'r')
grid
xlabel('micrometers');
ylabel('Amplitude');
hold on;

% Envelope generation through Hilbert Transformation
H=hilbert(sF);
Envelope=abs(H);

% Filtering of the Envelope using a low pass filter
filter_cutoff2=0.2;
fF=my_filter(Envelope, dz, filter_cutoff2);
```

```

% Plotting the Envelope on the graph of the intensity variation
plot(z,fF,'b')
hold on

% Determination of the maxima of the envelope
maxpeaks = zeros(1,2);
maxlocs = zeros(1,2);

[peaks,locs]=findpeaks(fF);
for j=1:2

    maxpeaks(1,j) = max(peaks);
    val=maxpeaks(1,j);
    pos=find(peaks==val);

    maxlocs(1,j) = locs(1,pos);

    peaks=peaks(peaks~=maxpeaks(1,j));
    locs=locs(locs~=maxlocs(1,j));
end

zpercentage=maxlocs/num_images;
zlocation=zpercentage*total_microns;
plot(zlocation,maxpeaks, 'r*');

toc

```

## Full 3D Code

```

clear; clc; close all;
tic

% Opening the images and setting piezo travel distance
num_images=954; % Set by the video being analyzed
total_microns=80; % Total travel of the piezo for this test

Vid=openLVVid('practice_vid_100micron_530_f145_cerulean1.lvvid');
VidReordered=openLVVid('practice_vid_100micron_530_f145_cerulean1.lvvid.reordered'); % Speeds up analysis, ask Ellery if confused on how it works
Image_stack=zeros(1,num_images);

Frame_num1=zeros(Vid.imageHeight,Vid.imageWidth);
Frame_num1(:)=NaN;
Frame_num2=zeros(Vid.imageHeight,Vid.imageWidth);
Frame_num2(:)=NaN;
z=(total_microns/num_images):(total_microns/num_images):total_microns;
dz=(total_microns/num_images);

```

```

Slice_frame1=zeros(num_images, Vid.imageWidth);
Slice_frame1(:)=NaN;
Slice_frame2=zeros(num_images, Vid.imageHeight);
Slice_frame2(:)=NaN;

filter_cutoff=(1/(2*dz))-0.001;
filter_cutoff2=0.2;

%Use the first set if looking to analyze entire field of view, second if
%you want to define a smaller window

N1=1; N2=Vid.imageWidth;   dy=Vid.imageWidth;
N3=1; N4=Vid.imageHeight;  dx=Vid.imageHeight;

% N1=530; N2=559; dy=30;
% N3=250; N4=279; dx=30;

for y=N1:N2 %Vid.imageWidth
    for x=N3:N4 %Vid.imageHeight

        Image_stack=getLVVidPixelallReordered(VidReordered,y,x,
Vid.imageWidth, Vid.numFrames);

        % Plot of Intensity Variation and Envelope Generation

        % Measure the intensity axially along a pixel
        Intensity=(Image_stack);
        A=Intensity(:);
        s=detrend(A);

        % Envelope generation through Hilbert Transformation
        H=hilbert(s);
        Envelope=abs(H);

        % Filtering of the Envelope using a low pass filter
        fF=my_filter(Envelope, dz, filter_cutoff2);

        % Finds the 2 peaks
        maxpeaks = zeros(1,2);
        maxlocs = zeros(1,2);

        [peaks,locs]=findpeaks(fF);
        for j=1:2

            maxpeaks(1,j) = max(peaks);
            val=maxpeaks(1,j);
            pos=find(peaks==val);

            maxlocs(1,j) = locs(1,pos);

            peaks=peaks(peaks~=maxpeaks(1,j));
            locs=locs(locs~=maxlocs(1,j));
        end
    end
end

```

```

zpercentage=maxlocs/num_images;
zlocation=zpercentage*total_microns;

Frame_num1(y,x)=zlocation(1,1);
Frame_num2(y,x)=zlocation(1,2);

if x==round(((N4-N3)/2)+N3)
    for k=3:num_images-1;

        I1=A(k-2,1);
        I2=A(k-1,1);
        I3=A(k,1);
        I4=A(k+1,1);

        I0=(I1+I2+I3+I4)/4;

        G=sqrt((((I3-I2)^2)+((I1-I2)^2))/(sqrt(2)*I0));

        Slice_frame1(k,y)=G;
    end
end

if y==round(((N2-N1)/2)+N1)
    for l=3:num_images-1;

        I1=A(l-2,1);
        I2=A(l-1,1);
        I3=A(l,1);
        I4=A(l+1,1);

        I0=(I1+I2+I3+I4)/4;

        G=sqrt((((I3-I2)^2)+((I1-I2)^2))/(sqrt(2)*I0));

        Slice_frame2(l,x)=G;
    end
end

if (mod(x,10) == 0)
    strcat('x=',num2str(x),'y=',num2str(y))
end
end
end

% Delete data if too noisy, has to be done manually
frame_num11=Frame_num1;
% frame_num11(frame_num11>=105)=NaN;
% frame_num11(frame_num11<=60)=NaN;

frame_num22=Frame_num2;
% frame_num22(frame_num22>=110)=NaN;
% frame_num22(frame_num22<=70)=NaN;

Distance1=frame_num11;

```

```

Distance2=frame_num22;
pixel_size=6.45; %Microns
magnification=5; % Magnification of the objective lens, x times
Xfieldofview=(pixel_size*dx)/magnification;
Yfieldofview=(pixel_size*dy)/magnification;
Dx=(Xfieldofview/dx);
Dy=(Yfieldofview/dy);
x_axis=Dx:Dx:Xfieldofview;
y_axis=Dy:Dy:Yfieldofview;
z_axis=3*dz:dz:total_microns-4*dz;

[X,Y]=meshgrid(x_axis,y_axis);

[X1,Z]=meshgrid(x_axis,z_axis);

Slice1=Slice_frame1(3:num_images-4,N1:N2);
Slice2=Slice_frame2(3:num_images-4,N3:N4);

M=Distance1(N1:N2,N3:N4);
N=Distance2(N1:N2,N3:N4);

mi=min(N);
mimi=min(mi);
ma=max(M);
mama=max(ma);

% Setting up fake surface to be able to plot image
ximage1=[0 Xfieldofview; 0 Xfieldofview];
yimage1=[Yfieldofview/2 Yfieldofview/2;Yfieldofview/2 Yfieldofview/2];
zimage1=[-mama -mama;-mimi -mimi];

ximage2=[Xfieldofview/2 Xfieldofview/2;Xfieldofview/2 Xfieldofview/2];
yimage2=[0 Yfieldofview;0 Yfieldofview];
zimage2=[-mama -mama;-mimi -mimi];

surf1(X,Y,-M) % Surface plot of the data
hold on
surf1(X,Y,-N)
hold on
shading interp
colormap(bone);
xlabel('x axis (microns)');
ylabel('y axis (microns)');
zlabel('depth (microns)');

SliceOut1=Slice1(mama/dz:mimi/dz,:);
SliceOut2=Slice1(mama/dz:mimi/dz,:);

surf(ximage1,yimage1,zimage1,'CData',SliceOut1,'FaceColor','texturemap')
surf(ximage2,yimage2,zimage2,'CData',SliceOut2,'FaceColor','texturemap')

toc

```

# Labview Code

